

Cosmic-ray driven outflow from the galactic center and the origin of magnetized radio filaments

F. Yusef-Zadeh^{1*} & M. Wardle²

¹*CIERA, Department of Physics and Astronomy Northwestern University, Evanston, IL 60208*

²*Dept of Physics and Astronomy, Research Centre for Astronomy, Astrophysics and Astrophotonics, Macquarie University, Sydney NSW 2109, Australia*

Accepted XXX. Received YYY; in original form ZZZ

ABSTRACT

Radio, X-ray and infrared observations of the inner few hundred pc of the Galactic center have highlighted two characteristics to the ISM. The cosmic ray ionization rate derived from molecular ions such as H_3^+ , is at least two to three orders of magnitudes higher than in the Galactic disk. The other is bipolar X-ray and radio emission away from the Galactic plane. These features are consistent with a scenario in which high cosmic ray pressure drives large-scale winds away from the Galactic plane. The interaction of such a wind with stellar wind bubbles may explain the energetic nonthermal radio filaments found throughout the Galactic center. Some of the implications of this scenario is the removal of gas driven by outflowing winds, acting as a feedback to reduce the star formation rate in the central molecular zone (CMZ), and the distortion of azimuthal magnetic field lines in the CMZ to vertical direction away from the plane. The combined effects of the wind and vertical magnetic field can explain why most magnetized filaments run perpendicular to the Galactic plane. This proposed picture suggests our Milky Way nucleus has recently experienced starburst or black hole activity, as recent radio and X-ray observations indicate.

Key words: accretion, accretion disks — black hole physics — Galaxy: center

1 INTRODUCTION

MeerKAT observations of the Galactic center have recently discovered a spectacular bubble of radio emission at 1.3 GHz extending over 430pc (Heywood, et al. 2019). This bubble covers prominent radio continuum sources such as the radio arc at $l \sim 0.2^\circ$, Sgr C at $l \sim -0.5^\circ$, nonthermal radio filaments (NRFs), and the radio lobes showing a mixture of warm ionized, dust and synchrotron emission (Sofue & Handa 1984; Tsuboi, et al. 1995; Bland-Hawthorn, & Cohen 2003; Yusef-Zadeh et al. 2004; Law et al. 2009; Alves et al. 2015; Nagoshi et al. 2019). Radio recombination line (RRL) observations of warm ionized gas in the northern and southern lobes show velocities ranging between ~ 20 and -20 km s^{-1} , respectively (Alves et al. 2015). The MeerKAT bubble appears to be filled with hot coronal X-ray gas (Nakashima, et al. 2013; Nakashima, Koyama & Wang 2019; Ponti et al. 2019) indicating that an energetic outflow took place few times $10^5 - 10^6$ years ago. These structures are distributed in the inner 75pc of the Galaxy where high cosmic ray ionization rate has been inferred, as discussed below. The trig-

gering event is likely to be enhanced accretion onto the $4 \times 10^6 M_\odot$ black hole, Sgr A*, or a burst of star formation activity or both that took place few times $10^5 - 10^6$ years ago (e.g. Alexander 2012; Zubovas & Nayakshin 2012; Wardle & Yusef-Zadeh 2014).

H_3^+ absorption measurements toward more than 30 stellar sources indicate that the Galactic center cosmic ray ionization rate (ζ) is higher than in diffuse or dense clouds in the Galactic disk by two or three orders of magnitudes, respectively (e.g. Geballe, et al. 1999; Oka, et al. 2005; Indriolo & McCall 2012; Goto, et al. 2014; Oka, et al. 2019). Detailed modeling yields $\zeta = 2 \times 10^{-14} \text{ s}^{-1}$ (Oka, et al. 2019) and $(1 - 11) \times 10^{-14} \text{ s}^{-1}$ (Le Petit et al. 2016). These high values explain three important characteristics of the gas in this region.

One, cosmic ray heating explains the pervasive distribution of warm molecular gas ($T \sim 75\text{-}200\text{K}$) compared to the $20 - 30\text{K}$ dust temperature throughout the Galactic center (Pierce-Price, et al. 2000), a result of heating by cosmic rays (Güsten et al. 1981; Yusef-Zadeh, Wardle & Roy 2007).

Two, cosmic ray interactions with the ISM produce a significant fraction of the steady and variable components of FeI K_α line emission at 6.4 keV in the Galactic center (Yusef-Zadeh, et al. 2007, 2013).

* E-mail: zadeh@northwestern.edu

Three, nonthermal bremsstrahlung produced by GeV cosmic ray electrons interacting with neutral gas produces the γ -ray emission detected by Fermi. Compelling evidence for this mechanism is the observed broken power law spectrum of γ -ray emission which is consistent that seen in the radio spectrum (Yusef-Zadeh, et al. 2013). In this picture, the γ -ray flux is proportional to the product of gas density and nonthermal radio flux. The average gas density estimated from fitting γ -ray data is similar to that found from H_3^+ measurements, less than 100 cm^{-3} (Yusef-Zadeh, et al. 2013; Oka, et al. 2019). This agreement confirms that most of the gas in the inner 2° by 1° of the Galactic center is filled by warm, diffuse, low density gas clouds and that dense gas has low volume filling factor (Oka, et al. 2019).

Here, we examine the origin of extended coronal gas, nonthermal radio filaments and vertical magnetic fields, all extending away from the plane and arising because of over-pressured cosmic rays in the CMZ driving an outflow.

2 COSMIC RAY DRIVEN WINDS

Cosmic rays drive winds in the nuclei of galaxies (Kulsrud & Cesarsky 1971; Zweibel 2017, and references therein). They also play a role in feedback, limiting star formation and the growth of the central supermassive black holes by transferring their momentum and energy into the surrounding medium. Here we interpret the large scale X-ray and synchrotron emission above and below the CMZ as emission arising from a cosmic-ray driven outflow, as drawn schematically in Figure 1 (e.g. Breitschwerdt, et al. 1991; Everett, et al. 2008; Everett, Schiller & Zweibel 2010; Ruzkowski et al. 2017). We also explain the origin of warm ionized gas and dust along the eastern and western edges of the bubble as the consequence of coronal gas pushing the warm ionized gas mixed in with dust in the direction where the lobes of the bubble lie, $l \sim 0.2^\circ$ and $\sim -0.5^\circ$, extending up to a degree away from the Galactic plane. The high energy density of cosmic rays $\geq 10^3 \text{ eV cm}^{-3}$ in the Galactic center suggests global injection of relativistic particles into the CMZ by an energetic event such as black hole activity or due to multiple supernova explosions. The MeerKAT bubble and the bipolar X-ray features are likely relics of this event (Heywood, et al. 2019).

Cosmic-ray driven outflow has been used to explain thermal X-ray and synchrotron emission from the inner few kpc of the Galaxy (Everett, Schiller & Zweibel 2010). In this picture, the cosmic rays momentum and energy are mediated by the magnetic field and are transferred to accelerating and heating the gas. Mass loss from the inner ~ 2 -3 kpc of Galactic disk has been estimated by fitting the X-ray and synchrotron emission indicating that gas and cosmic ray pressures launch a wind (see Fig. 5 of Everett, Schiller & Zweibel 2010). The best joint fit to the soft X-ray and radio synchrotron emission yields a pressure $\sim 5.5 \times 10^4 \text{ cm}^{-3} \text{ K}$ at the base of the wind (Everett, Schiller & Zweibel 2010). We are considering a similar scenario except that it is on the 300 pc scale of the bipolar X-ray emission and warm ionized gas in the MeerKAT bubble. The radio bubble and X-ray chimney features lie at the base of a much larger scale structure, the well-known "Fermi bubbles", where out-flowing gas has been detected symmetrically on a scale of

a few kpc away from the Galactic plane (Su et al. 2010; Yang et al. 2013). Recent analysis of Fermi data suggests excess γ -ray emission on a scale similar to MeerKAT bubble (Heywood, et al. 2019; Herold, & Malyshev 2019). The X-ray and synchrotron sources are likely to be scaled-down version of an outburst activity that produced the Fermi bubbles. (Nakashima, Koyama & Wang 2019; Ponti et al. 2019; Heywood, et al. 2019).

Here we examine whether the observed bremsstrahlung emission from the coronal gas in chimneys, warm ionized gas peaking in the lobe and radio synchrotron emission are consistent with a cosmic-ray driven wind scenario.

We note that both γ -ray and H_3^+ measurements indicate a low average gas density in the CMZ. This may be the result of a wind driven outflow removing the gas to high altitudes and regulating star formation in the CMZ. However, the high value of ζ suggests that past nuclear activity may have been more likely in removing gas from the disk of the Galaxy by inducing a wind rather than an outburst of star formation.

Assuming a 10% helium to hydrogen ratio by number and full ionization, the pressure of the thermal X-ray plasma is $P_g/k \approx 1.3 \times 10^6 \text{ K cm}^{-3}$, the thermal energy density $U_g = \frac{3}{2}P_g \approx 170 \text{ eV cm}^{-3}$, density $\rho \approx 2 \times 10^{-25} \text{ g cm}^{-3}$ and the sound speed around 400 km s^{-1} . Similarly, thermal RRL emission gives the gas pressure $P_g/k \approx 3.8 \times 10^6 \text{ K cm}^{-3}$ with energy density $U_g \approx 490 \text{ eV cm}^{-3}$.

The cosmic-ray pressure P_c in the wind, should be compatible with that needed to maintain the elevated cosmic-ray ionization rate of $\zeta_H = 10^{-14}$ - 10^{-13} s^{-1} in the CMZ that has been inferred from stellar H_3^+ absorption measurements (Oka, et al. 2019). In the solar neighborhood, the interstellar cosmic-ray energy density of 1.8 eV cm^{-3} produces $\zeta_H \approx 3 \times 10^{-17} \text{ s}^{-1}$ (Webber 1998), implying that cosmic-ray energy density in the CMZ 500 - 5000 eV cm^{-3} at the base of the wind. We expect the value in the wind to be somewhat lower depending on the scale height of the wind, so we adopt $U_c = 1000 \text{ eV cm}^{-3}$, implying a cosmic-ray pressure $P_c/k = \frac{1}{3}U_c/k \approx 3.9 \times 10^6 \text{ K cm}^{-3}$.

To estimate the magnetic field strength, we use the observed intensity of the synchrotron emission from the chimney at 4.8 GHz (Law, Yusef-Zadeh & Cotton 2008), i.e. $I_\nu \approx 0.5 \text{ Jy}$ per 153 arcsec FWHM beam, and standard, if somewhat uncertain, assumptions about the population of cosmic ray electrons: their energy density is 2% of the total in cosmic-rays, i.e. 20 eV cm^{-3} with an E^{-2} power law running between 1 MeV and 100 GeV, and that the depth of the source, L is the same as the transverse extent on the sky, i.e. 150 pc. The synchrotron intensity is then computed using $I_\nu = j_\nu L$, with j_ν the synchrotron emission coefficient for a power-law electron spectrum (e.g. Rybicki & Lightman 1979), yielding:

$$I_\nu \approx 0.144 \frac{e^3 B}{m_e c^2} E_\nu n(E_\nu) L, \quad (1)$$

where $n(E) dE$ is the number density of cosmic-ray electrons in the energy range $[E, E + dE]$, and

$$E_\nu = \left(\frac{4\pi m_e c \nu}{3eB} \right)^{1/2} m_e c^2 \quad (2)$$

is the characteristic energy of the electrons radiating significantly at frequency ν . With these assumptions we obtain $B = 4.3 \mu\text{G}$, an order-of-magnitude below the equiparti-

tion value of $39 \mu\text{G}$. This implies a magnetic energy density $U_B \approx 0.46 \text{ eV cm}^{-3}$, Alfvén speed $v_A \approx 27 \text{ km s}^{-1}$, characteristic electron energy $E_\nu \approx 8.3 \text{ GeV}$, and a synchrotron loss time 54 Myr .

The total pressure $\approx 5.2 \times 10^6 \text{ K cm}^{-3}$, is an order of magnitude greater than the upper envelope of the range considered in the models of [Everett, Schiller & Zweibel \(2010\)](#), but, this is compensated by the density in the X-ray chimney being 20 times larger than in the winds they consider. Neglecting the magnetic field, the sound speed in the cosmic ray dominated medium is $c_* = ((5P_g + 4P_c)/\rho)^{1/2} \approx 720 \text{ km s}^{-1}$, indicating that the medium is able to expand well away from the Galactic plane, but may not escape the Galaxy. The inferred outflow rate is $\dot{M} = 2\pi r^2 \rho c_* \approx 0.075 M_\odot \text{ yr}^{-1}$, where $r \approx 75 \text{ pc}$ is the cylindrical radius of the chimney. If the medium expands away from the plane, the origin of outflow driven lobes and Fermi bubbles may be related to each other. The inferred pressure of cosmic rays significantly exceeding the thermal pressure is consistent with cosmic ray driven Galactic wind simulations ([Salem, & Bryan 2014](#); [Ruszkowski et al. 2017](#)).

Bipolar hollow lobe of warm ionized gas surrounds the region where coronal gas is detected. The temperature and rms density $< n_e^2 >^{1/2}$ derived for this gas are $T_e \approx 4000 \text{ K}$ and $\approx 10 \text{ cm}^{-3}$, respectively ([Law et al. 2009](#); [Nakashima, Koyama & Wang 2019](#)). However collisional broadening of the higher-frequency recombination lines implies much higher densities, $n_e \sim 300 - 1000 \text{ cm}^{-3}$, consistent with pressure equilibrium with the coronal gas, and implying volume filling factor $\sim 10^{-4}$ for this material ([Law et al. 2009](#)).

The bulk of the material in the lobe or the northern half of the bubble is traced by mid-infrared dust emission from a $5 \times 10^6 M_\odot$ neutral medium with mean density $n_H \sim 300 \text{ cm}^{-3}$ ([Bland-Hawthorn, & Cohen 2003](#)) and shell thickness 5 pc , yielding a surface density $\Sigma_{\text{shell}} \sim 0.01 \text{ g/cm}^2$. If the internal bubble of coronal gas is over pressured with respect to the exterior, it is accelerating the shell at a rate $P_{\text{tot}}/\Sigma_{\text{shell}} \sim 20 \text{ pc Myr}^{-2}$. This is consistent with models in which the expanding bubble has swept up the shell within the last 3 Myr .

We next consider how the presence of this wind may explain the nonthermal radio filaments.

3 NONTHERMAL RADIO FILAMENTS (NRFS)

Radio observations have identified a system of magnetized filamentary structures and large-scale radio bubble within the inner two degrees of the Galactic center and vertical lobes at the edges of the bubble (e.g. [Yusef-Zadeh, Morris & Chance 1984](#); [Yusef-Zadeh, et al. 1986](#); [Yusef-Zadeh et al. 2004](#); [Sofue & Handa 1984](#); [Heywood, et al. 2019](#)). Over the years dozens of long and narrow linear filaments have been found with aspect ratio of 10-100 ([Liszt 1985](#); [Gray, et al. 1991](#); [Haynes, et al. 1992](#); [LaRosa, et al. 2004](#); [Yusef-Zadeh, et al. 1986](#); [Yusef-Zadeh et al. 2004](#); [Lang, Morris & Echevarria 1999](#); [Law, Yusef-Zadeh & Cotton 2008](#)). They appear as isolated, or bundled filaments running parallel to each other. The magnetic field is aligned along the linear

filaments and is mainly directed perpendicular to the Galactic plane ([Inoue, et al. 1984](#); [Tsuboi, et al. 1995](#); [Yusef-Zadeh, Wardle & Parastaran 1997](#)).

The morphology shows that the lobes and the magnetized linear filaments as two main components of a coherent structure. The lobes coincide with the edge-brightened structure of the MeerKAT bubble and almost all of the isolated and bundled linear filaments are distributed within the bubble. The new MeerKAT observations suggest strongly that the filaments and the lobes are causally connected to the origin of the radio bubble. The origin of NRFs that are found only in the Galactic center can now be understood in the context of their association with a unique event that produced the MeerKAT bubble ([Heywood, et al. 2019](#)).

A number of models have been proposed to explain the origin of the NRFs (see reviews by [Bicknell & Li 2001](#); [Ferrière 2009](#)). Two models that we focus here use stellar interactions with the ISM ([Nicholls & Le Strange 1995](#)) and the interaction of a Galactic wind with a cloud ([Shore & LaRosa 1999](#); [Dahlburg, et al. 2002](#); [Banda-Barragán, et al. 2016](#)). These models address three key questions related to the filamentation structure: 1) The mechanism that accelerates particles to GeV energies, 2) why certain filaments are detected and not others if there is a global mechanism for their production, and 3) why the magnetic field structure runs mainly perpendicular to the Galactic plane, given that the magnetic field is azimuthal near the plane of the CMZ ([Nishiyama et al. 2010](#)).

3.1 Winds Interacting with Mass-losing Stellar Bubbles

One of the earliest models proposed that particles are accelerated to high energies at the termination shock of stellar wind bubbles ([Rosner & Bodo 1996](#)). In this scenario, the cosmic rays produced at the termination shock load onto pre-existing ordered magnetic fields surrounding the wind bubbles and produce static filamentary structures. One key aspect of this model is that the transverse size of the filament matches the size of stellar wind bubbles. An extension of this model was proposed by considering the collective winds of W-R and OB stars in a dense stellar cluster producing shock waves that accelerate particles to high energies ([Yusef-Zadeh 2003](#)). Another model suggested that the filament of the Snake filament is due to a runaway star intersecting a supernova remnant ([Nicholls & Le Strange 1995](#)) and leaving behind a trail of synchrotron emission. This model does not explain numerous other NRFs that are not associated with supernova remnants.

An alternative scenario that has been suggested is that the NRFs arise through the interaction of a cloud with the Galactic wind ([Shore & LaRosa 1999](#); [Dahlburg, et al. 2002](#); [Banda-Barragán, et al. 2016](#)). Numerical simulations show morphologies remarkably similar to the NRFs. The filaments are considered to be dynamic structures and the weak magnetic field is amplified locally without the need to invoke a large scale ordered magnetic field configuration ([Shore & LaRosa 1999](#)). In this picture, the magnetized wind advects the cloud and forms a current sheet in the wake behind the cloud with the filamentary structures resulting from shear-driven nonlinear instability ([Dahlburg, et al. 2002](#)). This picture is similar to the interaction the magne-

tized solar wind and a comet. 3-D MHD numerical simulations confirm the formation of a highly structured magnetotail (Gregori, et al. 2000). Cloud sizes are generally far larger than the width of the filaments, $\leq 5''$ (0.2pc).

Here we consider a hybrid model in which the magnetized filaments are produced at the interaction sites of the wind outflowing away from the Galactic plane and embedded stellar wind bubbles. However, unlike the original model in which a strong local ISM magnetic field is assumed to be perpendicular to the Galactic plane (Rosner and Bodo 1996), we assume that the weak magnetic field in the wind wraps around the stellar wind bubble and forms a long tail behind the star (see Fig. 2). The outflowing galactic center wind and its magnetic field are directed vertically away from the plane, but the horizontal component of the stellar orbital velocity means that magnetic field lines become draped over the stellar wind bubble (see Fig. 2). The combined thermal, cosmic-ray and ram pressure of the wind, $P_{\text{ext}}/k \approx 1.3 \times 10^7 \text{ K cm}^{-3}$ sets the stand-off distance r_w of the stellar wind termination shock:

$$r_w = \left(\frac{\dot{M}_w v_w}{4\pi P_{\text{ext}}} \right)^{1/2} \approx 0.17 \text{ pc} \quad (3)$$

where we have adopted stellar wind mass loss rates and wind speeds $\dot{M}_w = 1 \times 10^{-6} M_{\odot} \text{ yr}^{-1}$ and $v_w = 1000 \text{ km s}^{-1}$, respectively, and pushes the shocked stellar wind into a tail stretching in the direction of the wind.

Meanwhile, the wind's magnetic field is draped around the stellar bubble, and is stretched and compressed as the associated plasma is evacuated and flows upwards along the field lines, parallel to the tail of shocked stellar wind. This creates a filament with magnetic pressure equal to or a sizeable fraction of that in the surrounding cosmic-ray driven wind, i.e. $B \lesssim 210 f \mu\text{G}$, where $f \leq 1$ is the magnetic fraction of the total pressure.

This compressed field is the site of the synchrotron emission observed in the NRFs. The relativistic electrons responsible for the synchrotron emission may be residual cosmic-ray particles from the external wind that have not been expelled during compression of the magnetic field. Making the reasonable assumption that the cosmic-ray and magnetic pressures are equal and sum to P_{ext} yields intensity $48 \mu\text{Jy arcsec}^{-2}$ at 327 MHz for a source depth 0.3 pc, consistent with the observed filaments.

The stellar wind termination shock is another potential source of relativistic particles. For example, assuming cosmic-ray acceleration efficiency is 0.25 and the proton to electron ratio is 50:1, then the shock luminosity in relativistic electrons is $L_e = 0.005 \times \frac{1}{2} \dot{M}_w v_w^2$, i.e. $0.41 L_{\odot}$ for our adopted wind parameters. The electrons are advected away from the shock at the postshock speed, assumed to be $v_p = 100 \text{ km s}^{-1}$ (the adopted compression ratio of 10 is greater than for an adiabatic shock because of the transfer of energy to cosmic-ray particles), yielding an estimated postshock energy density $L_e / (4\pi r_w^2 v_p) \approx 27 \text{ eV cm}^{-3}$, comparable to the energy density in the magnetic draping scenario outlined in the previous paragraph. The origin of the increased compression ratio is not just the reduction in adiabatic index from $5/3$ towards $4/3$ due to the presence of relativistic particles (which would increase the compression ratio to 7 at most) but that the shock cools via particles escaping upstream (Helder et al. 2012). The postshock syn-

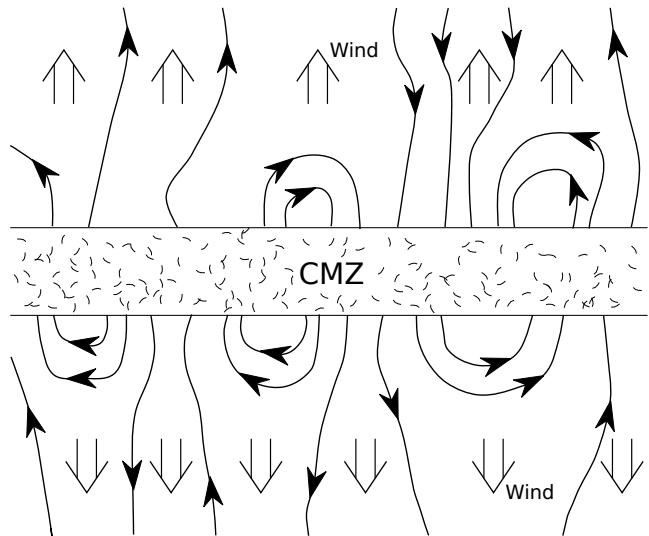


Figure 1. A large-scale schematic view of the CMZ azimuthal magnetic field getting distorted to vertical geometry by its interaction with the wind, launched by cosmic rays through the Streaming Instability.

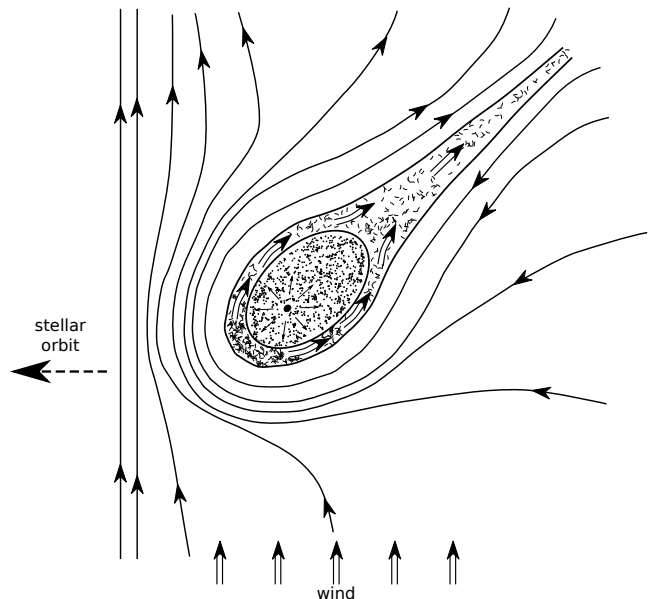


Figure 2. A schematic view of the interaction of the magnetized winds with a stellar bubble moving across the field lines

chrotron brightness is low, however, because the magnetic field there is largely self-generated by the cosmic-ray acceleration process and attains $\sim 1\%$ of the ram pressure i.e. $B \sim 20 \mu\text{G}$ (Helder et al. 2012). However this electron population may diffuse into the surrounding region of strong field and contribute significantly to the synchrotron emission from that region.

Although most NRFs show linear structure, a number of them deviate from this geometry. Some show kinks along their linear structures like the Snake (Gray, et al. 1991), or gently bend, deviating from straight lines perpendicular to the Galactic plane (Staguhn, et al. 1998; Yusef-Zadeh, et al. 2016) and some run approximately par-

allel to the Galactic plane (Lang, Morris & Echevarria 1999; LaRosa, Lazio & Kassim 2001). These variations in the morphology of NRFs can be understood in terms of wind driven outflows having different orientations that could vary as a function of time and different orbital velocities of stars. It is possible that the field lines are dragged so much that they get disconnected from their parent stellar wind bubble. In this scenario, there is no one-to-one association of filament and stellar wind bubbles. Unlike isolated filaments, a number of filaments are bundled and run parallel to each other (e.g., (Heywood, et al. 2019)). This network of filaments could be understood if the wind interacts with a cluster of mass-losing stellar wind bubbles. The best example of network of NRFs is found near where two well-known Arches and Quintuplet clusters of young stars lie. Alternatively, the network of filaments is a 2-D sheet- or cylindrical-like structure made up of individual filaments.

Two puzzling aspects of the nonthermal filaments are the mechanism responsible for accelerating particles to relativistic energies and the formation of elongated and narrow magnetized filaments, often consisting of multiple filaments running parallel to each other. There are no obvious compact sources that can eject relativistic particles and illuminate the jet-like appearance of elongated filaments. Here, we argued that the cosmic ray driven outflow away from the disk of the Galactic center is sweeping across embedded source. In analogy with the interaction of the solar wind interacting with the magnetic field of the Earth's atmosphere, we consider that outflow with a high cosmic ray pressure is interacting with the atmosphere of an embedded mass-losing star. We also discussed the origin of NRFs and why most of them run perpendicular to the Galactic plane. The wind can be produced globally and if the wind is related to Fermi Bubble outflows, it may be possible that additional NRFs are expected to be distributed away from the plane in the Fermi bubbles.

In summary, we discussed the consequences of high cosmic ray pressure in the Galactic center region and suggested that the coronal gas, the azimuthal magnetic field and the warm ionized gas are driven by an outflow. We also considered that Galactic center nonthermal radio filaments are generated by the interaction sites of wind driven Galactic center outflow and embedded stellar wind bubbles.

ACKNOWLEDGMENTS

This work is partially supported by the grant AST-0807400 from the the National Science Foundation.

REFERENCES

Alexander T., 2012, EPJWC, 5001, EPJWC..39
 Alves, M. I. R., Calabretta, M., Davies, R. D., et al. 2015, MNRAS, 450, 2025
 Banda-Barragán W. E., Parkin E. R., Federrath C., Crocker R. M., Bicknell G. V., 2016, MNRAS, 455, 1309
 Bicknell G. V., Li J., 2001, ApJ, 548, L69
 Bland-Hawthorn, J., & Cohen, M. 2003, ApJ, 582, 246
 Breitschwerdt D., McKenzie J. F., Voelk H. J., 1991, A&A, 245, 79

Dahlburg R. B., Einaudi G., LaRosa T. N., Shore S. N., 2002, ApJ, 568, 220
 Everett J. E., Zweibel E. G., Benjamin R. A., McCammon D., Rocks L., Gallagher J. S., 2008, ApJ, 674, 258
 Everett J. E., Schiller Q. G., Zweibel E. G., 2010, ApJ, 711, 13
 Ferrière K., 2009, A&A, 505, 1183
 Geballe T. R., McCall B. J., Hinkle K. H., Oka T., 1999, ApJ, 510, 251
 Goto M., Geballe T. R., Indriolo N., Yusef-Zadeh F., Usuda T., Henning T., Oka T., 2014, ApJ, 786, 96
 Gray A. D., Cram L. E., Ekers R. D., Goss W. M., 1991, Natur, 353, 237
 Gregori G., Miniati F., Ryu D., Jones T. W., 2000, ApJ, 543, 775
 Güsten, R., Walmsley, C. M., & Pauls, T. 1981, A&A, 103, 197
 Haynes R. F., Stewart R. T., Gray A. D., Reich W., Reich P., Mebold U., 1992, A&A, 264, 500
 Helder, E. A., Vink, J., Bykov, A. M., et al. 2012, Space Sci. Rev., 173, 369.
 Herold, L., & Malyshev, D. 2019, A&A, 625, A110
 Heywood I. et al. 2019, Nature, 10.1038
 Indriolo N., McCall B. J., 2012, ApJ, 745, 91
 Inoue M., Takahashi T., Tabara H., Kato T., Tsuboi M., 1984, PASJ, 36, 633
 Kulsrud R. M., Cesarsky C. J., 1971, ApL, 8, 189
 Lang C. C., Morris M., Echevarria L., 1999, ApJ, 526, 727
 LaRosa T. N., Lazio T. J. W., Kassim N. E., 2001, ApJ, 563, 163
 LaRosa T. N., Nord M. E., Lazio T. J. W., Kassim N. E., 2004, ApJ, 607, 302
 Law C. J., Yusef-Zadeh F., Cotton W. D., 2008, ApJS, 177, 515
 Law, C. J., Backer, D., Yusef-Zadeh, F., & Maddalena, R. 2009, ApJ, 695, 1070
 Le Petit, F., Ruaud, M., Bron, E., et al. 2016, A&A, 585, A105
 Liszt H. S., 1985, ApJ, 293, L65
 Nagoshi, H., Kubose, Y., Fujisawa, K., et al. 2019, PASJ, 71, 80
 Nakashima S., et al., 2013, ApJ, 773, 20
 Nakashima S., Koyama K., Wang Q. D., 2019, arXiv e-prints, arXiv:1903.11767
 Nicholls J., Le Strange E. T., 1995, ApJ, 443, 638
 Nishiyama, S., Hatano, H., Tamura, M., et al. 2010, ApJ, 722, L23
 Oka T., Geballe T. R., Goto M., Usuda T., McCall B. J., 2005, ApJ, 632, 882
 Oka T., Geballe T. R., Goto M., Usuda T., McCall B. J., 2019, ApJ, in press
 Pierce-Price D., et al., 2000, ApJ, 545, L121
 Ponti, G., Hofmann, F., Churazov, E., et al. 2019, Nature, 567, 347
 Rosner R., Bodo G., 1996, ApJ, 470, L49
 Ruszkowski, M., Yang, H.-Y. K., & Zweibel, E. 2017, ApJ, 834, 208.
 Rybicki G. B., Lightman A. P., 1979, rpa..book
 Salem, M., & Bryan, G. L. 2014, MNRAS, 437, 3312
 Shore S. N., LaRosa T. N., 1999, ApJ, 521, 587
 Staguhn J., Stutzki J., Uchida K. I., Yusef-Zadeh F., 1998, A&A, 336, 290
 Sofue Y., Handa T., 1984, Natur, 310, 568
 ()
 Su, M., Slatyer, T. R., & Finkbeiner, D. P. 2010, ApJ, 724, 1044
 Tsuboi M., Kawabata T., Kasuga T., Handa T., Kato T., 1995, PASJ, 47, 829
 Wardle M., Yusef-Zadeh F., 2014, ApJ, 787, L14
 Webber, W. R. 1998, ApJ, 506, 329
 Yang, H.-Y. K., Ruszkowski, M., & Zweibel, E. 2013, MNRAS, 436, 2734
 Yusef-Zadeh, F. 2003, ApJ, 598, 325.
 Yusef-Zadeh F., Morris M., Chance D., 1984, Natur, 310, 557
 Yusef-Zadeh F., Morris M., Slee O. B., Nelson G. J., 1986, ApJ, 310, 689

6 *Yusef-Zadeh & Wardle*

- Yusef-Zadeh F., Wardle M., Parastaran P., 1997, ApJ, 475, L119
Yusef-Zadeh, F., Hewitt, J. W., & Cotton, W. 2004, ApJS, 155, 421.
Yusef-Zadeh F., Muno M., Wardle M., Lis D. C., 2007, ApJ, 656, 847
Yusef-Zadeh F., Wardle M., Roy S., 2007, ApJ, 665, L123
Yusef-Zadeh F., et al., 2013, ApJ, 762, 33
Yusef-Zadeh F., et al., 2016, ApJ, 819, 60
Zubovas K., Nayakshin S., 2012, MNRAS, 424, 666
Zweibel E. G., 2017, PhPl, 24, 55402

This paper has been typeset from a $\text{\TeX}/\text{\LaTeX}$ file prepared by the author.